JOURNAL OF GEOPHYSICAL RESEARCH, VOL. 86, NO. C3, PAGES 2005-2016, MARCH 20, 1981

Thermally Driven Wind Variability in the Planetary Boundary Layer Above Lima, Peru

D. B. ENFIELD

School of Oceanography, Oregon State University, Corvallis, Oregon 97331

Land-sea thermal forcing of the coastal wind near Lima, Peru, is examined as a mechanism to explain the observed wind variability there, in particular the similarity between monthly anomalies of sea surface temperature and wind speeds on the interannual time scales typical of El Niño occurrences. Aerological and surface meteorological observations from Peru coastal sites are analyzed for two time scales: over 15–20 year periods (1958–1977) for monthly averaged data and over a year (1976–1977) for daily data. Wind profile characteristics and annual cycles, and their relation to the cross-coastal temperature gradient are qualitatively and quantitatively consistent with the thermally forced boundary-layer model proposed by Lettau (1978) to explain the Peru coastal wind. The cross-coastal air temperature difference between Lima and Callao explained 55% of the variance in the surface wind speeds at Lima during 1976–1977. The mean annual cycles of the surface wind at Lima and other Peru coastal locations are in phase with the annual solar heating cycle where the seasonality of low cloudiness is large but with the annual cycle of the southeast trade circulation where it is not. This suggests that insolation over the desert is the principal source of thermal forcing variability. During El Niño periods the alongshore wind and the cross-coastal circulation above Lima intensify, in conjunction with anomalously warm sea surface temperatures. The planetary boundary layer is destabilized, and the base of the winter inversion is eroded upward. The observations are consistent with a reduction of desert cloudiness during El Niño events owing to air-sea exchange and a consequent increase in the thermal forcing of the wind.

INTRODUCTION

Sea breeze circulations are a well-known consequence of the diurnally varying temperature contrast that develops between land and sea along coastlines. Differential daytime heating over the land results in the onshore flow of relatively cool air and the return flow of land-warmed air aloft, toward the sea. The maximum cross-coastal circulation occurs shortly after the maximum land-sea temperature contrast, and in the northern hemisphere the wind shifts to the right owing to the Coriolis effect [*Estoque,* 1961].

In the tropics, and in the mid-latitudes during summer, the contrary nocturnal phase may be less pronounced and the time-averaged system should retain the characteristics of the daytime effect: surface onshore flow, return flow aloft, and an alongshore component geostrophically balanced by the landward (steady state) pressure gradient associated with the thermal contrast. Conditions for such a mean air-land-sea system are ideal along the Peru coast, where coastal upwelling maintains a persistently cool ocean boundary. *Lettau* [1978] has developed a steady thermally forced model of the Peru coastal wind along these lines, in which an alongshore low level jet arises in the same sense (equatorward) as the regional SE trade circulation. The system is self-sustaining, because positive feedback exists between the thermal forcing and the upwelling.

The existence of a thermally forced low level jet along the Peru coast is poorly documented (Lettau had little direct evidence to support it). Moreover, the observation (see the next section) that the coastal winds become anomalously strong during years of abnormally warm sea surface temperatures (El Niño) runs contrary to the expected feedback relationship. The existence of a thermally forced low level jet and the mechanism for its increase during El Niño are the main topics of this paper.

WIND-SST RELATIONSHIPS DURING EL NIÑO

The occurrence during some years of anomalously warm sea surface temperature (SST) in the southeastern tropical Pacific—the phenomenon known as El Niño—has been attributed to a cessation or significant reduction of the southerly coastal winds off South America and of the upwelling they induce [*Wooster,* 1960; *Bjerknes,* 1966; *Caviedes,* 1973; *Wooster and Guillen,* 1974]. However, *Wyrtki* [1975] found that ship-reported winds off Peru (mostly from the coastal shipping lane) do not weaken during El Niño. He suggested, instead, that the SST departures arise from the anomalous advection of warm water from the midequatorial Pacific—an ocean relaxation owing to weakened winds in the central Pacific. Wyrtki's hypothesis that the relaxation takes the form of an eastward propagating, equatorially trapped internal Kelvin wave is supported by other recent studies [*McCreary,* 1976; *Hurlburt et al.,* 1976; *Kindle,* 1979; *Enfield and Allen,* 1980].

Wyrtki's work raises the question of what happens to the Peru coastal winds in association with El Niño. The *Enfield* [1980] analysis of the winds at Peru coastal airports confirms that the coastal wind remains upwelling favorable during El Niño. Moreover, the monthly anomalies of the wind at the Lima airport (12°S) are strongly and positively correlated with the local SST anomalies at Callao. The similarity between the anomalies of the Callao shore temperature and of the Lima wind speed can be seen in Figure 1. The high temperatures associated with El Niño coincide with periods of low Southern Oscillation Index (SOI), which is indicative of a weakened southeast trade circulation [*Quinn,* 1974]. The warm periods in 1957–1958, 1965, 1969, 1972–1973, and 1976 all have two anomaly maxima: the first near April–June, and the second near December–January. With the exception of 1965 the sequence of warm and cold years as well as the double peaks are reflected in the Lima wind speed. In 1965–1966, both the positive anomalies and the double peaks occurred in the 950 mbar wind, suggesting that erroneous surface wind data exist for that year. Thus the entire atmospheric

Paper number 80C1340.
0148-0227/81/080C-1340$01.00

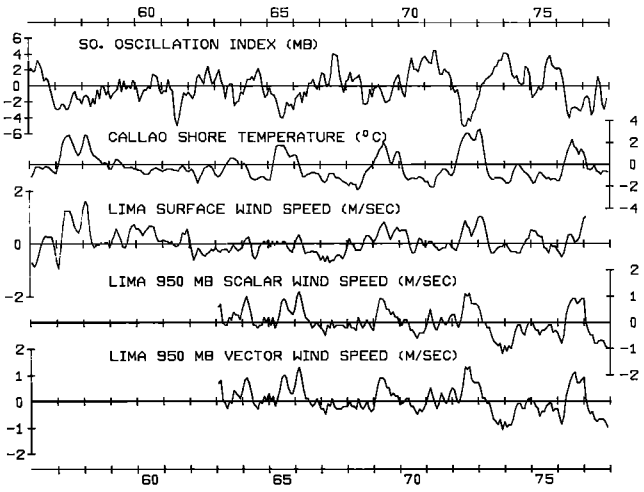

Fig. 1. Three-month running mean time series of monthly anomalies of the Southern Oscillation Index (difference in atmospheric pressure between Easter Island and Darwin, Australia); the Callao shore temperature; the scalar surface wind speed at Lima; and the scalar and vector wind speeds at 950 mbar (about 500 m) above Lima. Years are indicated along the abcissa.

boundary layer above Lima probably behaved similarly during all the El Niños since 1955.

It may be that the regional atmospheric circulation of the southeastern tropical Pacific strengthens during El Niño, in contrast to the mid-Pacific trades, and that the Lima wind merely reflects this tendency. But this would not agree with indications that the south Pacific anticyclone weakens [e.g., *Quinn*, 1974], nor would it explain the mimicking of details in the Callao SST anomalies. The latter feature suggests that SST anomalies somehow force the Lima wind anomalies; two mechanisms for this seem plausible. First, enhanced mixing in the marine boundary layer owing to warm surface conditions could increase the downward eddy transport of momentum from a stronger circulation aloft. At Lima this is not possible because the wind maximum occurs at low levels, within the mixed layer, where anomalies are in the same sense as at the surface (i.e., the entire low level flow increases during El Niño).

A more likely mechanism for the SST-wind correlations evident in Figure 1 is an increased onshore-offshore pressure gradient owing to an enhanced cross-coastal thermal contrast between land and sea. In this paper I will first demonstrate that the mean profile at Lima and its fluctuations at time scales of a few days to 1 year are consistent with a dynamical model of thermal forcing of the wind by a land-sea air temperature gradient. I will subsequently show how such thermal forcing can explain the observed relationship between the interannual anomalies of the Lima wind and the Callao SST.

OBSERVATIONS

The observations were made at the locations shown in Figure 2. Daily 00 GMT (1900 local) rawinsonde data from the Lima airport, digitized at 50 mbar intervals of pressure, were obtained from the National Climatic Center for the period from October 1957 through December 1977. The 00 GMT sampling time appears to be satisfactory, because the Peru alongshore wind is best developed in the late afternoon and in the early evening [*Burt et al.*, 1973; *Lettau*, 1978]. Monthly averages were computed for air temperature, potential temperature, relative humidity, vapor pressure, speed, direction, and directional steadiness.

The first 63 months of rawinsonde data were not considered for this study because of a 9-month data gap and internal inconsistencies that indicate data quality problems. For the remaining 15-year time series (1963–1977), it was only necessary to make two adjustments. Linear interpolation was used to fill a 1-month gap (July 1971). Also, the station site had been changed in April 1967, the elevation changing from 135 to 13 m. Hence, biases appeared for some time series between the

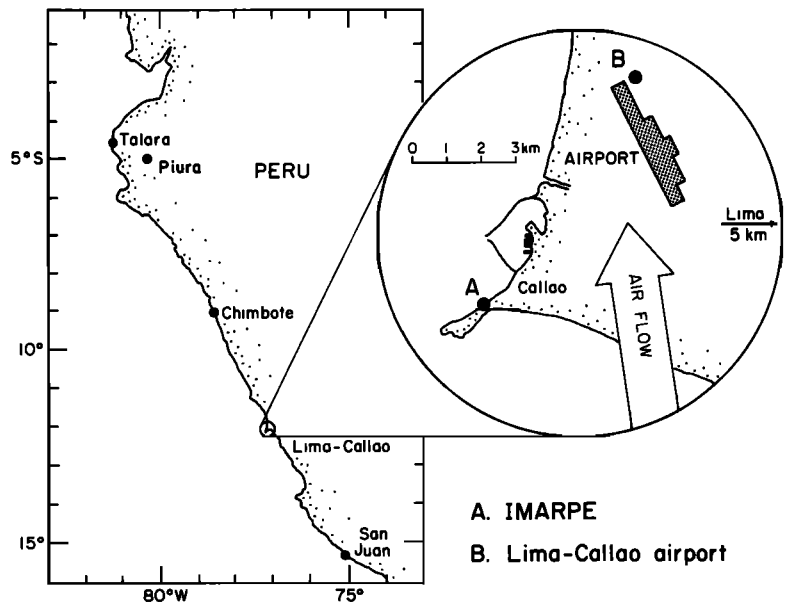

Fig. 2. Locations of observation sites.

period before and after the change. The affected time series before relocation were made compatible with the present site by addition or subtraction of the differences in mean values for the two periods.

Surface (scalar) wind speeds at the Lima airport, based on hourly anemometer measurements, were obtained from the Corporacion Peruana de Aviacion Civil (CORPAC) for two time scales: monthly averaged from 1949 to 1978, and daily averaged for 1976 to 1977. Daily averaged air temperatures were also obtained from CORPAC for the latter period. The 950 mbar rawinsonde data in Figure 1 suggest clearly that the Lima wind is very steady, such that scalar speeds, $(\overline{U^2 + V^2})^{1/2}$, provide a reasonable estimate of vector speeds, $(\bar{U}^2 + \bar{V}^2)^{1/2}$, and the alongshore component. The scalar and vector speeds at 950 mbar (about 500 m height) have a correlation of 0.98. Monthly values of the directional steadiness of the wind were computed as the ratio (expressed in percent) of the mean scalar speed to the mean vector speed. The 15-year average directional steadiness is 86%. The steadiness is even higher for the surface (95%) and 1000 mbar (96%) levels. Such directional steadiness is typical for the Peru coast [*Prohaska*, 1973].

From May 20, 1976, through May 19, 1977, air temperatures were recorded hourly by an Aanderaa data logger on top of the 25-m high Instituto del Mar (IMARPE) building in La Punta, Callao, as part of the Joint 2 upwelling experiment of the Coastal Upwelling Ecosystems Analysis program (CUEA). This site is located on a coastal spit of land that intercepts the marine air flow from the ocean, about 8 km shoreward from the airport station (Figure 2). The hourly temperatures were daily averaged and were increased by a constant amount (determined from average lapse conditions) to make the mean values at 25 m comparable to the surface values at Lima.

Anomalies of monthly data were extracted by calculating the mean values for each of the 12 months of the year to form the annual cycle and by subtracting the latter from the data by corresponding months. All daily averaged data from 1976–1977 were smoothed with a 3-day running mean (3 DRM). This effectively eliminated variability on time scales at or less than the local inertial period, which is about 2.4 days. The SSE-NNW (150°–330°T) direction, which is very close to the coastline orientation from 11°S to 13°S, was used to decompose rawinsonde wind data into cross-coastal (U) and alongshore (V) velocity components, positive onshore and equatorward, respectively.

BOUNDARY-LAYER MODEL

The Peru coastal wind is characterized by a low-level alongshore wind jet with its maximum strength in the atmospheric boundary layer below one kilometer [*Lettau and Rutllant-Costa*, 1978]. *Lettau* [1978] argued that the time-averaged jet is primarily driven by the thermal contrast between the cool ocean littoral and the warmer coastal desert. Both the temperature contrast and the associated pressure gradient decrease with height. The result is a surface intensified alongshore geostrophic wind, which combines with frictional effects near the surface to produce the low level jet, centered approximately over the coastline. Thermodynamic considerations require a cross-coastal (ageostrophic) circulation to transport ocean-cooled air landward near the surface and export desert-warmed air seaward aloft.

To represent the mean jet, *Lettau* [1978] proposed a steady state model of the planetary boundary layer with uniform eddy viscosity, temperature (density)* that decays exponentially with height (z), and a horizontal temperature gradient that varies as a gaussian in the cross-coastal direction (x). A similar exponential thermal wind problem was previously solved by *Mahrt and Schwerdtfeger* [1970] to model boundary layer flow over the Antarctic Plateau. Applying a zero transport constraint to the vertically integrated cross-coastal flow, *Lettau* [1978] arrived at the following expressions for the onshore (U) and alongshore (V) wind profiles at the coast ($x = 0$):

$$U(\zeta) = \tfrac{1}{3}|V_{0g}|e^{-\zeta}\,[3 \sin \zeta + \cos \zeta - \exp(\zeta/2)] \qquad (1)$$

and

$$V(\zeta) = \tfrac{1}{3}V_{0g}e^{-\zeta}\,[\sin \zeta - 3 \cos \zeta + 3 \exp(\zeta/2)] \qquad (2)$$

where $\zeta = z/H$ and H is a scale height. The constant V_{0g} is the alongshore surface geostrophic wind at the coast and is given by

$$V_{0g} = -\frac{gT^*H}{L\langle T\rangle f} \qquad (3)$$

where g is the acceleration owing to gravity, L is the cross-coastal scale of the thermally forced system, T^* is the temperature difference scale corresponding to L, $\langle T\rangle$ represents the surface air temperature averaged over L, and f is the Coriolis parameter ($\approx -0.3 \times 10^{-4}$ s^{-1} at Lima). The scale height (H) is such that $H^2 = 2K/|f|$, where K is the effective kinematic eddy viscosity.

Lettau did not verify the model with aerological observations. But using reasonable values of L (50–100 km), T^* (3°–6°C), and H (400–800 m), he obtained the essential features known to exist in the Peru coastal wind: a jet core in the lower kilometer, onshore flow in the first few hundred meters above the ground and offshore flow from there to 1000–1500 m

TABLE 1. Annual Mean Values of Constant Pressure Height (Z_p, Geopotential Meters), Vector Speed (S), Vector Direction (Ø), and Directional Steadiness (D.S.) for Constant Pressure Levels Above Lima (The Annual Mean Potential Temperature Gradient (θ_z) Between Levels is Also Shown.)

	Constant Pressure Level, mbar						
	SFC	1000	950	900	850	800	750
Z_p, gpm	13	102	540	1001	1490	2006	2551
S, m s^{-1}	4.3	4.4	3.0	0.4	0.4	0.3	0.3
Ø, °T	165	167	145	99	150	358	101
D.S., percent	95	96	86	36	30	37	37
θ_z, °C/km)	4.5	10.5	11.7	7.2	5.6	4.8	

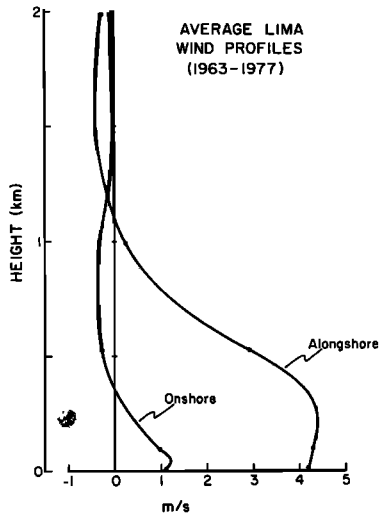

Fig. 3. Long-term mean vertical profiles of the onshore and alongshore wind components at Lima, Peru (1963–1977). Dots indicate the mean heights of the 50-mbar rawin observations used.

height. Moreover, when combined with an ocean Ekman spiral, the model yielded a reasonable thermodynamic energy balance for the air-sea-land system.

Long-Term Mean Conditions

Table 1 summarizes the overall mean values of a number of pertinent variables derived from the 50-mbar rawinsonde data for the period 1963–1977. The mean profiles of the onshore (U) and alongshore (V) wind are drawn in Figure 3. The mean distributions of air temperature (T), vapor pressure (P_v), and component velocities by constant pressure level and time of year are contoured in Figure 4. (The even spacing of levels does not seriously distort the true pressure-height distribution except between 1000 mbar and the surface; refer to the mean heights from Table 1.)

Prominent features of the temperature and water vapor distributions (Figure 4) include a strong subsidence inversion near 950–850 mbar that usually sets in about May and persists until November without interruption. Temperature and moisture at lower levels reach minimum values in August (owing to lower SST, winds, and insolation) and maxima in February. *Prohaska* [1973] found that the winter inversion extends typically from about 700 to 1500 m, with a near normal lapse rate from the surface to the inversion base. During the summer, smaller and less permanent inversions occur mostly below 500 m, owing to the combined effects of subsidence and oceanic cooling. As a result the air below the winter inversion is probably less stable than for the same layer in the summer. According to *Prohaska* [1973] the nearly uninterrupted cloudiness over Lima in winter (June–October) consists of a stratus layer extending from ceiling heights of 150–300 m to the inversion base. The strong inversion traps moisture in the surface layer where relative humidities of 80–90% are typical, and the cloudiness is formed and is maintained primarily by a mixing condensation process. In the summer (December–April) the relative humidities in the first several hundred meters reach a minimum (70–80%) because air temperatures are higher and the vapor flux, though also greater, is allowed to extend to much higher levels. Summer fogs form offshore along upwelling fronts and are driven toward the coast by early morning onshore winds. The fog transforms into low stratocumuliform cloudiness which usually dissolves by midday as the wind increases and backs to a more nearly alongshore direction.

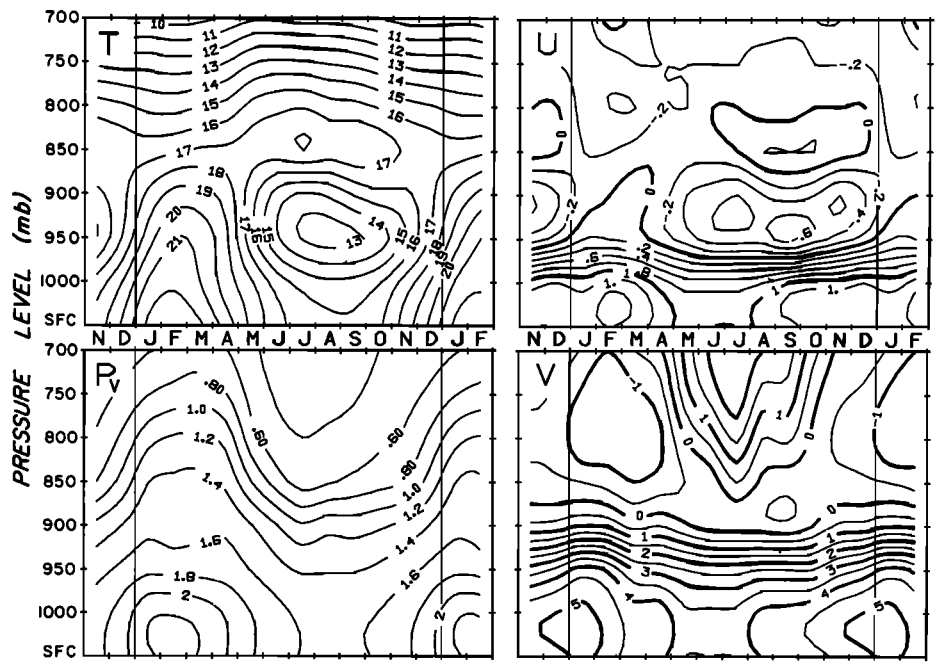

Fig. 4. Contoured sections of the mean annual cycles of air temperature (T, °C), vapor pressure (P_v, mbar), onshore velocity (U, m s^{-1}) and alongshore velocity (V, m s^{-1}) above Lima, Peru, for the period 1963–1977, plotted by months of the year and by pressure level. The mean heights of the rawin pressure levels are given in Table 1.

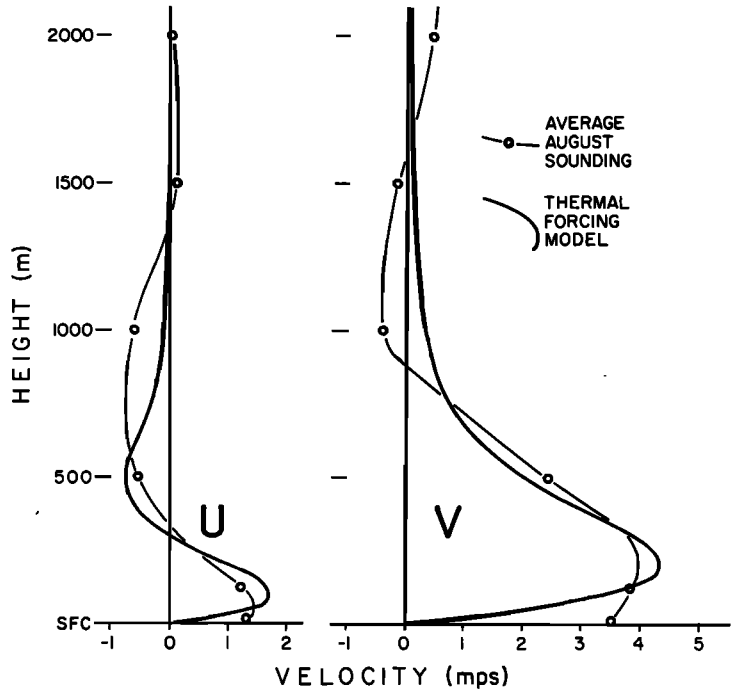

Fig. 5. Mean August vertical profiles of the onshore (U) and alongshore (V) components of the wind above Lima, Peru, shown with the corresponding profiles from the *Lettau* [1978] model, using (1) and (2) with $V_{0g} = 8$ m s^{-1}, $H = 160$ m. Circles indicate the mean heights of the 50 mbar rawin observations used.

The vector wind speed at Lima (Figure 4) is greatest from the surface to 950 mbar and decreases rapidly from the inversion base (near 950 mbar) to only 10% of near-surface values in the 900–750 mbar layer (see Table 1, Figure 4). The resultant direction is from the southeast in the surface layer, nearly coast-parallel but with an onshore component. The surface layer winds vary little in direction during the year but become about 40% stronger in January–February than in June–July.

The contour plots (Figure 4) show that the wind is jet-like in the vertical and suggest that the alongshore maximum occurs somewhere near 1000 mbar, from 50 to 200 m in height, while the onshore maximum occurs lower, possibly below 100 m. Within the winter inversion there is a marked layer of offshore flow from at least May–December centered near the 900 mbar level (Figure 4). In the summer months the maximum offshore component becomes more diffuse in the vertical, centered near 800 mbar.

The model profiles for U and V as functions of the height (z) are shown in Figure 5, using $V_{0g} = 8$ m s^{-1} and $H = 160$ m, together with the average Lima rawinsonde profiles for August. The principal features of the data are reasonably reproduced, except for the shear in the first 100 m above the ground and the thickness of the offshore flow aloft. The similarity of the mean data to Lettau's model and the absence of significant alongshore flow above 1 km suggest that thermal forcing

TABLE 2*a*. Annual Cycles of Inland Air Temperatures (T_a), Coastal Sea Surface Temperatures (T_s), the Temperature Differences ($\Delta T = T_a - T_s$), the Relative Differences ($\Delta T/\overline{\Delta T}$), and the Wind Speeds ($W$) at 12°S. (Each Average is Computed for the Period 1958–1977, Inclusive)

Month	T_a, °C, Lima	T_s, °C, Callao	ΔT, °C	$\Delta T/\overline{\Delta T}$	W, m s^{-1}, Lima
January	21.6	16.6	5.0	2.2	4.0
February	22.2	17.4	4.8	2.1	3.5
March	21.8	17.9	3.9	1.7	3.2
April	20.2	17.4	2.8	1.2	3.1
May	18.4	17.1	1.3	0.6	2.7
June	17.0	16.6	0.4	0.2	2.6
July	16.2	16.1	0.1	0.0	2.7
August	15.9	15.8	0.1	0.0	2.9
September	15.9	15.3	0.6	0.3	3.2
October	16.7	15.1	1.6	0.7	3.4
November	18.2	15.5	2.7	1.2	3.5
December	20.0	15.9	4.1	1.8	3.9

TABLE 2*b*. Annual Cycles of Inland Air Temperatures (T_a), Coastal Sea Surface Temperatures (T_s), the Temperature Differences ($\Delta T = T_a - T_s$), the Relative Differences ($\Delta T/\overline{\Delta T}$), and the Wind Speeds ($W$) at 5°S (Each Average is Computed for the Period 1958–1977, Inclusive)

Month	T_a, °C Piura	T_s, °C, Talara	ΔT, °C	$\Delta T/\overline{\Delta T}$	W, m s^{-1}, Talara
January	27.0	20.6	6.4	1.1	7.5
February	28.1	21.6	6.5	1.1	6.4
March	28.2	21.3	6.9	1.2	6.0
April	27.1	19.9	7.2	1.3	7.7
May	25.2	19.0	6.2	1.1	9.2
June	23.3	18.5	4.8	0.8	9.7
July	22.1	18.0	4.1	0.7	9.5
August	22.2	17.6	4.6	0.8	9.4
September	22.3	17.6	4.7	0.8	9.6
October	22.8	17.8	5.0	0.9	9.4
November	23.8	18.0	5.8	1.0	9.1
December	25.4	18.4	7.0	1.2	8.8

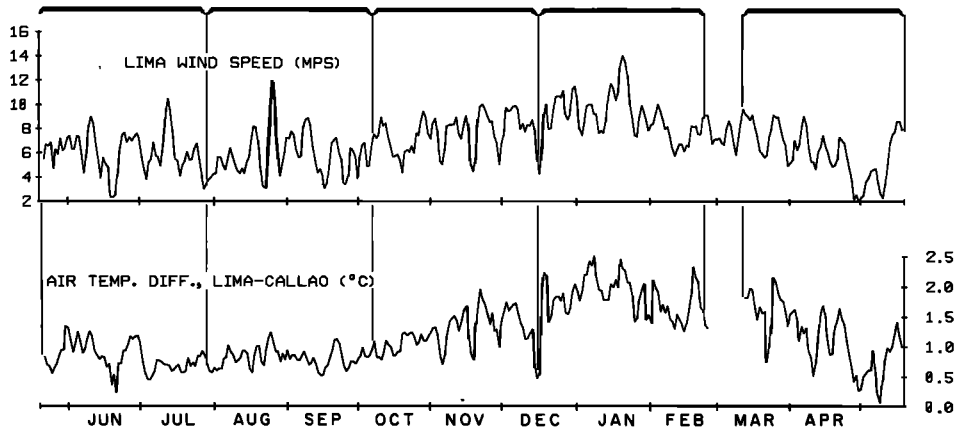

Fig. 6. Three-day running mean time series of daily averages of the (top) scalar surface wind speed at the Lima airport and the (bottom) air temperature difference between the airport and IMARPE, from May 20, 1976, through May 19, 1977. Brackets indicate the data segments used in separate correlation analyses. Geographic locations are shown in Figure 2.

is perhaps the most important factor governing the behavior of the Peru coastal wind.

It should be noted that the annual cycle of the winds at Lima is out of phase with the southeast (Pacific) trades documented by *Wyrtki and Meyers* [1976]. The Lima wind maximum occurs in January, 1 month before the local heating maximum (Figure 4), whereas the southeast trades are strongest in July-August-September. Thus the annual wind cycle is in much better agreement with the heating cycle than with the trade circulation.

The annual cycles of wind speeds and temperatures at various coastal locations indicate the probable importance of seasonal cloudiness in controlling the relative influence of thermal forcing and trade circulation (seasonally) on coastal winds. At Lima (12°S), where the winter cloud cover is most prevalent, the thermal contrast between land and sea is much greater during the relatively cloud-free summer season than during the winter months. The difference between the air temperature at Lima and the sea surface temperature at Callao undergoes a large annual oscillation that corresponds well to that of the Lima wind (Table 2*a*). Near 5°S, stratiform winter cloudiness is rare, and the seasonality of cloud cover is much less marked than at 12°S. Accordingly, the difference between the air temperature over the Sechura Desert (Piura) and the sea surface temperature at Talara has a much smaller seasonal oscillation relative to its mean (Table 2*b*). Thus the seasonality of thermal forcing is less important, and the annual cycle of wind speed agrees with that of the trade circulation. At Chimbote (9°S), where winter low clouds are common (as at Lima), and at San Juan (15°S), where they are not, wind speeds reach their maximum in the summer and winter, respectively.

1976–1977 Period

The year-long record of air temperature from the IMARPE building in Callao, from May 20, 1976, through May 19, 1977, (henceforth the '1976–1977 year'), made it possible to compute crosscoastal air temperature differences (ΔT) between Lima and Callao for that period. The relationship between ΔT and the Lima wind is described below and compared with the *Lettau* [1978] model, both for the annual means and the fluctuations. The time series are shown in Figure 6, and the geographic relationship between measurement sites is shown in Figure 2.

Annual means. Figure 5 shows that the Lettau wind profile as a whole is representative of the averaged Lima wind profiles, but that details of the data, for example, the surface wind or near-surface shear, are not well reproduced. The time average of the vertical integrals of the alongshore wind profiles should provide a stable quantity with which to test the thermal forcing model. Integrating (2) from the surface to some height (h),

$$I_v(h) = (V_{0_g}H/3)\exp(-h/H)[\cos(h/H) - 2\sin(h/H) - 6\exp(H/2H)] + 5V_{0_g}H/3 \quad (4)$$

For sufficiently large heights the alongshore wind becomes negligibly small, and the integral (4) approaches the limiting value $I_v = 5V_{0_g}H/3$. By using (3), the relation between the profile integral and the cross-coastal temperature gradient scale, Γ, becomes

$$I_v = 1852\,\Gamma\,H^2 \quad (5)$$

where $g = 10\ \mathrm{m\ s^{-2}}$, $f = -0.3 \times 10^{-4}\ \mathrm{s^{-1}}$, $\langle T\rangle = 300°\mathrm{K}$, and $\Gamma = T^*/L$.

The alongshore rawinsonde profiles were numerically integrated from the surface to 800 mbar and the integrals averaged for the 1976–1977 year to yield the estimate $\bar{I}_v \simeq 3160\ \mathrm{m\ s^{-1}}$ (the overbar denotes a time average). If L is assigned the mesoscale order of 100 km and T^* the representative range of 3°–7°C, then the surface temperature gradient scale (Γ) will have the range 0.03–0.07°C/km^{-1}. The actual pointwise surface temperature gradient will be a maximum at the coastline, considerably above the scale value, Γ. From (5) the corresponding range for $\bar{H}$ is 160–340 m. Thus observations and theory combine to give an estimate of a few hundreds of meters for the exponential scale height, which is consistent with the wind profiles shown in Figures 3–4.

Periodicities of a year or less. It is not possible to use the rawinsonde profiles in the above manner to investigate the wind variability, because individual profiles are instantaneous samples subject to aliasing and large sampling errors. They cannot

TABLE 3. Quantities Related to the Correlation Between the Wind Speed (S) at Lima and the Air Temperature Difference (ΔT) Between Lima and Callao

Segment†	r	r/σ	τ	b	r^2	$r^2-\sigma^2$
Year	0.76	4.3*	14	3.61	0.58	.55
1	0.47	2.2	3.2	3.39	0.22	.17
2	0.50	3.0	2.0	5.51	0.25	.22
3	0.61	3.2	2.5	3.05	0.37	.33
4	0.66	3.7	2.1	3.49	0.44	.41
5	0.74	3.3	3.2	3.47	0.55	.50

The symbols r, σ, τ, and b represent the zero lag correlation, the large lag standard error, the independence time scale (days), and the regression coefficient of S on ΔT (m s^{-1} °C^{-1}).

*An upper limit, since the necessary integration for σ could not be carried far enough (τ is underestimated).

†The 70-day segments are successively numbered as discussed in the text.

be satisfactorily treated to yield stable values of I_v with an effective time scale of variability similar to the filtered surface wind speeds and temperatures. Therefore, the variable portions of the surface wind speed and thermal gradient were compared directly from the 1976–1977 data set. This is based on the assumption that the surface wind speed (S) should be linearly related to I_v. Regression of I_v from individual profiles on the daily averaged wind speeds yielded $\hat{I}_v = 590\ S$ (means and linear trends removed). The correlation coefficient, 0.35, was significant at above the 99.9% level (all significance tests for correlations follow the method outlined by *Sciremammano* [1979]).

The procedure used was the following. First, the filtered time series of Lima wind speed and air temperature difference (Figure 6) were lag correlated for the entire year (the missing Callao temperatures in February–March 1977 were compensated for by letting $\Delta T = 0$ for those days and by reducing the number of observations correspondingly). The two series were then divided into five 70-day segments, and each segment was similarly correlated. Linear trends were removed from all time series (year and segments) prior to correlation. Finally, the wind speed (S) was regressed on ΔT for each of the six cases.

A byproduct of the lagged correlations is the calculation of the integral time scale of variability (τ) and the large-lag standard error (σ) as defined and discussed by *Davis* [1976] and *Sciremammano* [1979], respectively. The time scale, τ, is also known as the independence time scale because it is an estimate of the time interval for which successive bivariate pairs may be considered statistically independent. The large-lag standard error, σ, is a measure of the inherent error in the correlation estimates (i.e., the correlation to be expected owing only to random associations between the two variables). The normalized correlation, r/σ, is simply related to the correlation significance and is more meaningful than the raw correlations because it does not depend on either τ or the number of observations. Values of $r/\sigma = 1.7$, 2.0, 2.6, and 3.3 are equivalent to the 90, 95, 99, and 99.9% significance levels, respectively, assuming bivariate normality. The apparent skill of a time series regression is r^2, the artificial skill is σ^2, and the true skill is $r^2 - \sigma^2$ [*Davis*, 1976].

The time series of S and ΔT are similar both in their annual cycles and for their variability on time scales of days to weeks (Figure 6). Table 3 summarizes the pertinent quantities for each of the cases considered. In all cases the maximum correlation occurred at zero lag, although the correlation function was always skewed such that at a 1 day lag the correlation for ΔT leading S was greater than for S leading ΔT. Only the first 70-day segment was not significant at above the 99% level, while the average significance of segments 2–5 was 99.9%. The average of the true skills for the 70-day segments is 33%, while the true skill for the year is 55% (the 'average' of several correlation skills is meaningful here, since the segment

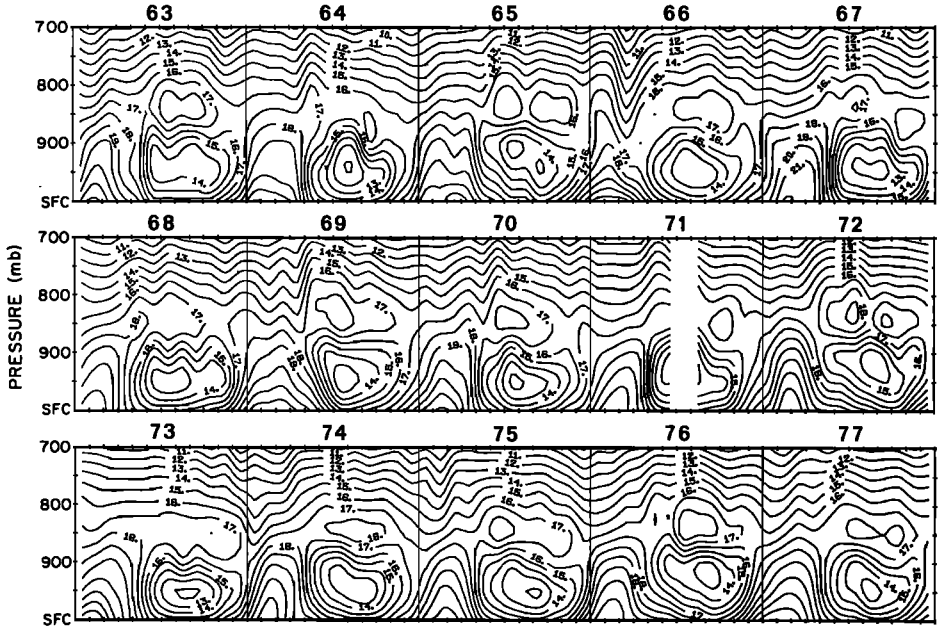

Fig. 7. Contoured section of the monthly averaged air temperature above Lima, plotted by time and by pressure level for the period 1963–1977. The mean heights of the rawin pressure levels used are given in Table 1.

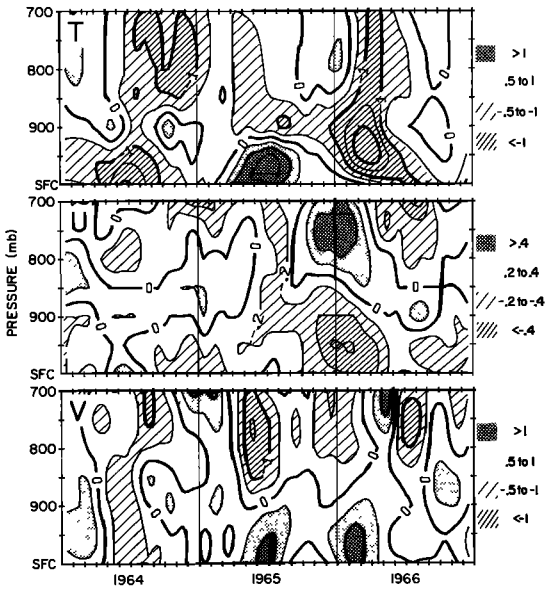

Fig. 8. Contoured sections of the monthly anomalies of air temperature (T, °C), onshore velocity (U, m s^{-1}), and alongshore velocity (V, m s^{-1}) above Lima, Peru, plotted by time and by pressure level for the period 1964–1966. The mean heights of the rawin pressure levels used are given in Table 1.

variances did not differ greatly). Hence 22% of the total variability in S is effectively explained by variability in ΔT at periodicities of about several months to a year, while 33% is explained at periodicities of several days to several months. These figures constitute only one yearly sample and are subject to unknown errors if taken as estimates of the same percentages over many years. Clearly, however, a significant relationship exists, and it may be concluded that thermal forcing is well related to the wind variability over Lima over time scales of days to 1 year.

A rule of thumb in numerical work is that differencing enhances errors. In the absence of a dynamical relationship involving the temperature difference, this leads one to expect that either of the two temperatures alone (Lima or IMARPE) would be as well correlated with S, or better, than ΔT. However, the correlation between S and ΔT is about twice as large, on the average, as is S with either of the two temperatures alone, although all correlations are positive. Hence the cross-coastal temperature difference appears to be inherently significant in respect of the wind variability, rather than a reflection of other relationships involving the (undifferentiated) temperature.

Quantitative consistency. A simple scale analysis of the wind data indicates that the local time derivative of the onshore wind (U_t) is 1 order of magnitude smaller than the Coriolis term (fV) at the inertial frequency (and smaller still at lower frequencies). Hence the filtered data shown in Figure 6 should be in a quasi-steady balance, and it should be possible to compare the response of S to ΔT with that expected from the steady *Lettau* [1978] model.

A reasonable approach is to let the variable alongshore jet profile be represented by (2) with a time dependent geostrophic wind, $V_g(t)$, in place of the constant V_{0g}. Then,

$$V_g(t) = R_s\Delta T(t) = V_{0g}\Delta T(t)/\overline{\Delta T} \qquad (6)$$

where R_g is the geostrophic response, $\Delta T(t)$ is the time variable temperature difference between two points separated in the cross-coastal sense (and $\overline{\Delta T}$ its time average), and V_{0g} is the average (constant) geostrophic wind as defined by (3).

In his example, *Lettau* [1978] used scale parameters which lead to $V_{0g} = 21$ m s^{-1}, a value that overestimates the mean aerological profile at Lima. To obtain the reasonably good fit to mean data shown in Figure 5, the value $V_{0g} = 8$ m s^{-1} was used. The mean temperature difference between Lima and Callao for the 1976-1977 year was 0.94°C, after accounting for the difference in observation heights. These figures lead to an estimated (model) geostrophic response of 10–20 m s^{-1} °C^{-1}, whereas the observed response of the surface wind speed was 3.1–5.5 m s^{-1} °C^{-1} (Table 3). This yields a ratio of surface to geostrophic wind of about 0.2–0.5, which is not unreasonable. Therefore, the observed response of the Lima wind to the cross-coastal temperature gradient is quantitatively consistent with the *Lettau* [1978] thermal forcing model.

In summary, both the means and variabilities of the observations are qualitatively and quantitatively consistent with Lettau's model of thermal forcing of the Peru coastal wind. The similarities between theory and observation are remarkable, considering how idealized *Lettau*'s [1978] Ekman model is (e.g., since the model assumes a height-independent kinematic eddy viscosity where a strong inversion is known to exist).

Interannual Variability

For the period 1963–1977 there is no way to parameterize the cross-coastal temperature gradient as was done for 1976–1977, because only the Lima air temperatures are available. On the interannual time scale the Lima air temperatures are positively correlated with wind speeds (using anomalies), and the anomalies of air temperature also behave similarly to anomalies of SST, both being positive during El Niño periods. The approach adopted in this section is to examine qualitatively the interannual behavior of the lower atmosphere over

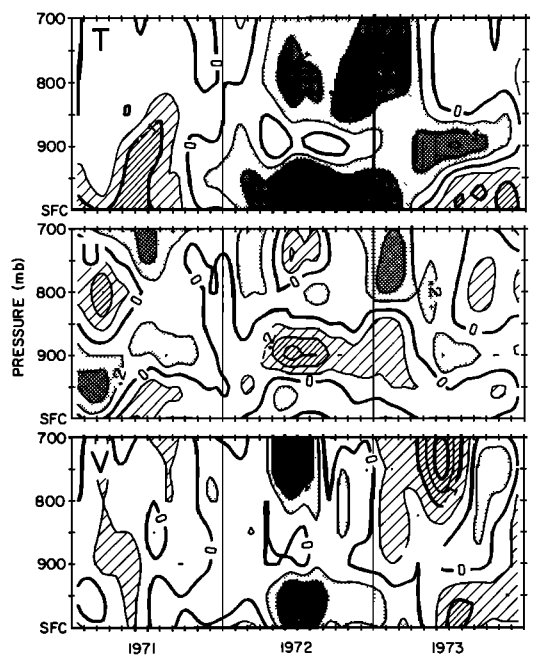

Fig. 9. As in Figure 8, for the period 1971–1973.

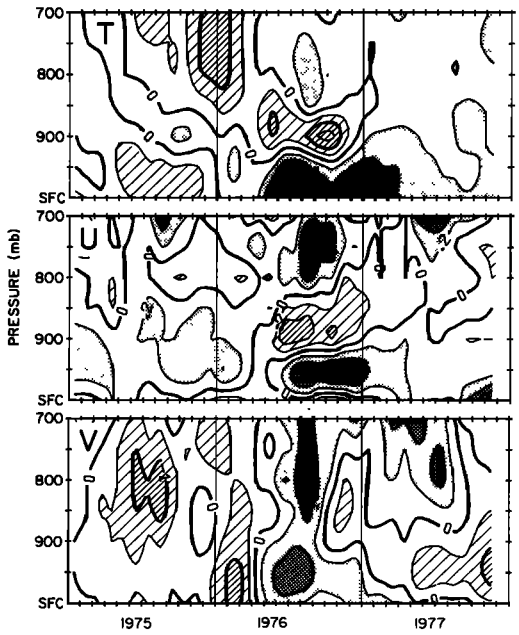

Fig. 10. As in Figure 8, for the period 1975–1977.

Lima, and, with the aid of results on annual and within-year variability (previous two sections), surmise the processes which may result in wind speed increases during El Niño.

Figure 7 shows the 15-year distribution of air temperature in the lower atmosphere above Lima. The principal features of the average distribution (Figure 4) are present every year. In particular, the winter inversion is always present, roughly from 950 to 850 mbar and from May to November, during all Niño events (1965, 1972, 1973). Two anomalous features occur during El Niño periods. The first of these is the warmer air found between the surface and 900 mbar and lasting from about May of the onset year (e.g., 1972) through February of the following year (compare with the average, Figure 4). This can be seen more clearly in the anomaly sections of Figures 8–10.

A second feature in Figure 7 is the tendency for the inversion base to be found somewhat higher during El Niño, roughly between 950 and 900 mbar rather than near 950 mbar, as in most years (see, e.g., 1965, 1972, 1976). It is difficult to detect a similar rise in the top of the inversion (850 mbar), however. The approximate temperature difference of 5°–6°C between the base and top of the inversion does not change significantly from year to year, although both temperatures tend to be near or slightly above the average during El Niño years. The principal difference in the inversion appears to be at the inversion base, which is about 200–300 m higher during El Niño.

Figures 8–10 show the distributions of anomalous temperature, onshore wind, and alongshore wind during the 3-year periods spanning the 1965, 1972 and 1976 El Niño events, respectively. The anomalous distributions of temperature show additional details not apparent in Figure 7. There is a tendency for temperature to be lower than average during the years immediately preceding El Niño. This can also be seen in the SST anomalies (Figure 1). The largest positive anomalies during El Niño occur in the lowest 500 m (i.e., the subinversion layer from the surface to 950 mbar). Again, as with SST, there tend to occur two positive temperature anomaly peaks during each El Niño period. The largest is centered in June or July of the onset year (1965, 1972, 1976), lasts for 4 or 5 months and ranges from 2° to 3°C at the maximum. A second, less intense peak occurs in the subsequent December–January period. Another recurring feature is the colder than average temperature near 900 mbar during the winter months of the El Niño onset year. Together, the air temperature anomalies indicate that a significant destabilization occurs during El Niño in the first kilometer above Lima.

The most characteristic feature of the onshore wind component during El Niño is the intensification of the cross-coastal circulation, especially during the latter half of the onset year. In 1965 this was evidenced primarily by enhanced offshore flow near 900 mbar, in 1972 by anomalous onshore flow near 950 mbar, and in 1976 by both. As was with the inversion base, the anomalous offshore flow occurs at slightly higher levels than the average one shown in Figure 4.

It has already been noted that the surface wind speeds increase during El Niño and tend to have positive anomaly peaks concurrent with those of sea surface temperature. Figures 8–10 show that this behavior extends to almost 900 mbar for the alongshore component. During two events (1972, 1976), positive anomalies also occurred in the alongshore flow at higher levels (800–700 mbar) concurrently with the first low level anomaly peak.

One process that appears to take place during El Niño is increased mixing between the surface and 900 mbar. The cold anomalies near 900 mbar and warm anomalies below are evidence of destabilization owing to anomalous surface heating. The base of the inversion is apparently eroded upward as much as several hundred meters, suggesting that the cooler than normal air near 900 mbar may be a manifestation of increased mixing. The fact that the total temperature change across the inversion does not change much suggests that the anomalous mixing in the lower portion of the inversion is accompanied by increased subsidence aloft. Intensified subsidence aloft is also consistent with the somewhat warmer than normal temperatures above 850 mbar in 1965, 1972, and 1976 (Figures 8–10).

One source of anomalous surface heating is sensible heat transfer from the unusually warm sea surface, as can be seen from the shore temperature anomaly time series of Figure 11. During El Niño periods, both the sea surface and the Lima air temperatures are above normal, and the vapor pressures increase. The additional water vapor must come from the ocean and is brought landward by the net onshore component of the prevailing wind. Anomalous heat and moisture inputs at the surface both cause anomalous decreases in the stability. A clear reflection of this destabilization is the anomalous decrease of the potential temperature gradient from the surface to 900 mbar that occurs during El Niño events (Figure 11).

DISCUSSION

The link between the destabilization process (initiated by oceanic heating) and the wind speed increases observed during El Niño may be through solar heating (i.e., cloud cover). The climatology of Peru coastal cloudiness from Talara (4°S) to San Juan (15°S) seems to explain the annual wind cycles at various stations according to the seasonality of thermal forcing (see the section, Long-Term Mean Conditions). El Niño occurrences are known to be associated with anomalous rainfall and coastal flooding [e.g., *Caviedes,* 1973]. However, the

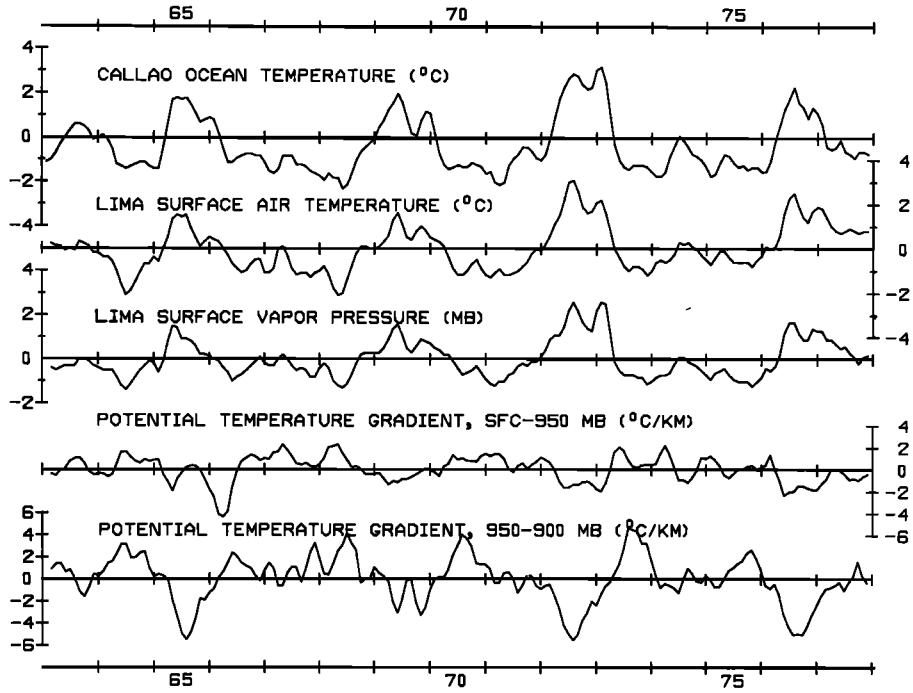

Fig. 11. Three-month running mean time series of monthly anomalies of the shore temperature at Callao and of various atmospheric variables at Lima, Peru. Positive potential temperature gradients correspond to greater than average stability for the layer indicated. Years are indicated along the abcissa.

rain is most prevalent north of about 8°S, associated with increased convective cloudiness. The rain in northern Peru may explain the decreases in the Talara wind during El Niño [*Enfield,* 1980], since the evaporation of anomalous land moisture would presumably reduce desert heating and therefore also thermal forcing of the wind [*Lettau,* 1978]. In contrast, the narrow coastal strip between 8°S and 14°S is but rarely affected by rain, even during El Niño events. In fact, I should acknowledge that my interest in the effects of the Peru cloudiness was first stimulated while living in Lima, where Peruvian scientists and local residents commented about the prolonged summer conditions and unusually sunny winter of 1972, a major El Niño.

The effect of a decrease in cloudiness should be to increase the land-sea thermal contrast. Because of its lower albedo, the ocean absorbs more of the radiation increase than does the desert. But the much greater thermal capacity of the ocean results in a significantly smaller surface temperature increase than is the case for the desert. This in itself would explain any increase in the cross-coastal thermal contrast associated with an increase of insolation. In addition, for the peculiar geometry of the Lima-Callao area (see Figure 2), the air flow from sea to land is such that the anomalous heating of the air over the desert is quickly superimposed on the heat already absorbed above the ocean surface, thus enhancing the thermal contrast still further. The end effect is an increase in the wind speed, given the validity of the thermal forcing mechanism.

If cloud dissipation over Lima is an important factor during El Niño, it may occur in one or both of two ways, depending mainly on season. During the winter, stratiform clouds form just below the inversion base where water vapor accumulates and the air temperature and dew point temperature are very nearly the same. As anomalous heating occurs in the subinversion layer and destabilization causes the inversion base to erode, the increase in saturation vapor pressure owing to warming and the decrease of vapor pressure owing to mixing of moist air in the cloud layer with the drier air above it tend to lower the relative humidity. However, an increased vapor flux from the warmer sea surface tends to raise the relative humidity. If the latter effect does not compensate for the former two, cloud dissipation should occur. Evidence for such dissipation comes from the decrease of relative humidity at the surface and at 1000 mbar during El Niño and the negative correlation of relative humidity anomalies with the Callao SST anomalies ($r = -0.53$ and -0.48 at the two levels, respectively). This is probably representative of conditions in the cloud layer above 1000 mbar because the entire subinversion layer tends to be well mixed in the winter [*Prohaska,* 1973]. (Note that examination of the relative humidity at 950 mbar is inappropriate, since that pressure surface is sometimes found above the inversion base, giving potentially misleading results.)

In the summer, morning low clouds form over Lima after the shoreward advection of fog [*Prohaska,* 1973] (see the section, Long-Term Mean Conditions). It was shown by *Zuta et al.* [1976] that during the 1972–1973 El Niño, warm SST anomalies resulted in negative air-sea temperature differences over much of the Peru coastal region. This reversal of the normally positive temperature difference would presumably inhibit fog formation, and therefore also the summer cloudiness. An indication that such dissipation occurs comes from minimum ceiling observations taken at the Lima airport before and during the 1976–1977 El Niño. In January-February-March 1976 (prior to the onset of El Niño conditions in April–May) 51 days with minimum ceilings of 300 m or less were reported, the average air temperature was 19.4°C and the average wind speed was 2.9 m s^{-1}. During the same period of 1977, only 13 days with minimum ceilings were reported,

while the average air temperature and wind speed were 23.2°C and 4.4 m s^{-1}, respectively. These figures are consistent with increased thermal forcing owing to the dissipation of summer cloudiness.

This paper presents several indications of destabilization in the lowest kilometer of the air column during El Niño events, which can be linked plausibly to an intensified coastal circulation through the thermal forcing mechanism and the dissipation of low stratiform clouds. The data are also very suggestive that these effects originate with an anomalously warm sea surface (e.g., Figure 1). Although the Peru coastal winds and upwelling persist during El Niño, it appears that anomalously warm water upwells owing to subsurface isotherm depression and anomalous advection [*Enfield,* 1980]. Maps of the air-sea temperature difference during the 1972–1973 El Niño suggest an abnormal sea-to-air sensible heat transfer immediately offshore of the upwelling zone (beyond 50–100 km) where the air flow is mainly alongshore [*Zuta et al.,* 1976]. Closer to the coast, where the wind has a stronger onshore component and the quasi-alongshore isotherms of SST are crossed in the downgradient sense, the air-sea temperature difference remains stable (positive). Thus it is not clear exactly how the destabilization of the lower atmosphere results from ocean surface effects.

The results of this study suggest that thermal forcing of the Lima wind may be operative at virtually all time scales from several days to interannual. This is paradoxical in view of the fact that at short time scales SST is negatively correlated with the local wind off Peru, as in other upwelling regions [*Brink et al.,* 1980], whereas at Lima the long time scale variabilities (annual and interannual) of SST and wind are positively correlated (Table 2*a*; Figure 1). There is a twofold explanation for this. First, SST is mainly responsive to the local wind (through the upwelling process) on the time scale of days to weeks, but to other factors, such as insolation and remotely forced advection, on the long time scales. Second, the role of cloudiness may be quite different at the long and short time scales, in terms of its relative importance and/or the way it is related to SST fluctuations.

Little can be said as to how the Peru coastal wind is related to the large-scale circulation of the southeast tropical Pacific, for which reliable data exist only at the annual frequency [e.g., *Wyrtki and Meyers,* 1976]. *Lettau*'s [1978] analysis, supported by this study, suggests that the thermally forced coastal jet should have a cross-coastal space scale of the mesoscale order of 100 km. *Brink et al.* [1980] found nearshore (6–12 km) and offshore (125 km) winds near 15°S to be coherent at most periodicities in the 2–15 day range. But buoy data are not available for the area off Callao (12°S), and the importance of thermal forcing may be quite different at the two latitudes.

While this study is very suggestive of the importance of thermal forcing along the Peru coast, it is severely limited by (1) the paucity of surface and upper air data in the alongshore and cross-coastal directions, (2) poor vertical resolution (50 mbar) and (3) a lack of data on insolation or cloudiness. Future studies of the Peru coastal wind should address these shortcomings, investigating in more detail the roles of sea surface temperature and cloudiness as well as the large space scale structure of the regional and coastal circulations.

SUMMARY AND CONCLUSIONS

The present study shows that thermal forcing is probably a significant, if not dominant, factor in the wind variability at Lima and that it provides a very plausible mechanism for explaining the anomalous wind increases observed during El Niño events. The principal results of this study can be summarized as follows:

1. The mean wind profile over Lima is characterized by a low level (50–200 m) alongshore jet and a cross-coastal circulation, in agreement with the thermal forcing model of *Lettau* [1978]. The vertically integrated mean alongshore flow is in quantitative agreement with the model.
2. At locations along the coast where winter low clouds are prevalent, the annual wind cycle is dominated by thermal forcing, and the maximum wind occurs in the austral summer. Where the seasonality of low clouds is small, the wind is maximum in the winter, in agreement with the SE trade circulation.
3. During 1976–1977, the cross-coastal air temperature gradient accounted for 55% of the annual and within-year variance of wind speed; the wind response was quantitatively consistent with *Lettau*'s [1978] thermal forcing model.
4. During the El Niños of 1965, 1972, and 1976, increased fluxes of heat and water vapor from the anomalously warm sea surface resulted in a destablization of the air column from the surface to about 1000 m; simultaneously, the inversion base rose about 200–300 m, apparently eroded by enhanced mixing. In addition to the low level (surface 950 mbar) increases in the alongshore wind, the cross-coastal circulation cell was intensified.

The characteristics of the planetary boundary layer over Lima during El Niño are consistent with the following scenario: (1) The anomalously warm ocean surface destabilizes the air column in the first kilometer above the ground, resulting in significant decreases in cloudiness; (2) increased insolation over the desert results in a greater cross-coastal air temperature gradient; and (3) the cross-coastal circulation cell and the alongshore jet are intensified owing to enhanced thermal forcing.

Acknowledgments. I am grateful to G. Belevan of the Corporacion Peruana de Aviacion Civil (CORPAC) for his assistance in obtaining much of the data used in this study. I also thank my colleagues C. Paulson, W. Quinn, K. Brink, and D. Stuart for their helpful discussions in relation to the work. This research was supported by National Science Foundation grant OCE 78-03382 as part of the Coastal Upwelling Ecosystems Analysis (CUEA) Program and also by National Science Foundation grant ATM 78-20419 of the Climate Dynamics Program.

REFERENCES

Bjerknes, J., Survey of El Niño 1957–58 in its relation to tropical Pacific meteorology, *Bull. Inter Am. Trop. Tuna Comm., 12,* 3–86, 1966.

Brink, K. H., D. Halpern and R. L. Smith, Circulation in the Peruvian upwelling system near 15°S, *J. Geophys. Res., 85,* 4036–4048, 1980.

Burt, W. V., D. B. Enfield, R. L. Smith, and H. Crew, The surface wind over an upwelling area near Pisco, Peru, *Boundary Layer Meteorol., 3,* 385–391, 1973.

Caviedes, C. N., Secas and El Niño: Two simultaneous climatical hazards in South America, *Proc. Assoc. Am. Geogr., 5,* 44–49, 1973.

Davis, R. E., Predictability of sea surface temperature and sea level pressure anomalies over the north Pacific Ocean, *J. Phys. Oceanogr., 6,* 249–266, 1976.

Enfield, D. B., El Niño: Pacific eastern boundary response to interannual forcing, in *Resource Management and Environmental Uncertainty: Lessons From Coastal Upwelling Fisheries,* edited by M. H. Glantz and J. D. Thompson, Interscience, New York, 1981.

Enfield, D. B., and J. S. Allen, On the structure and dynamics of monthly sea level anomalies along the Pacific coast of North and South America, *J. Phys. Oceanogr., 8,* 557–578, 1980.

Estoque, M. A., The sea breeze as a function of the prevailing synoptic situation, *J. Atmos. Sci., 26,* 82–95, 1962.

Hurlburt, H. E., J. C. Kindle, and J. J. O'Brien, A numerical simulation of the onset of El Niño, *J. Phys. Oceanogr., 6,* 621–631, 1976.

Kindle, J. C., Equatorial Pacific Ocean variability—Seasonal and El Niño time scales, Ph.D. dissertation, Florida State Univ., Tallahassee, 1979.

Lettau, H. H., Explaining the world's driest climate, in Exploring the World's Driest Climate, edited by H. H. Lettau and K. Lettau, *IES Rep. 101,* Univ. of Wisconsin, Madison, 1978.

Lettau, H. H., and J. Rutllant-Costa, Characteristic winds and boundary layer meteorology of the arid zones in Peru and Chile, in Exploring the World's Driest Climate, edited by H. H. Lettau and K. Lettau, *IES Rep. 101,* Univ. of Wisconsin, Madison, 1978.

Mahrt, L. J., and W. Schwerdtfeger, Ekman spirals for exponential thermal wind, *Boundary Layer Meteorol., 1,* 137–145, 1970.

McCreary, J., Eastern tropical ocean response to changing wind systems: With application to El Niño, *J. Phys. Oceanogr., 6,* 632–645, 1976.

Prohaska, F. J., New evidence on the climatic controls along the Peruvian coast, in *Coastal Deserts: Their Natural and Human Environments,* edited by D. H. K. Ameran and A. Wilson, University of Arizona Press, Tucson, 1973.

Quinn, W. H., Monitoring and predicting El Niño invasions, *J. Appl. Meteorol., 13,* 825–830, 1974.

Sciremammano, F., A suggestion for the presentation of correlations and their significance levels, *J. Phys. Oceanogr., 9,* 1273–1276, 1979.

Wooster, W. S., El Niño, *Rep. 7,* Calif. Coop. Oceanics and Fish. Invest., La Jolla, 1960.

Wooster, W. S., and O. Guillen, Characteristics of El Niño in 1972, *J. Mar. Res., 32,* 387–404, 1974.

Wyrtki, K., El Niño—The dynamic response of the equatorial Pacific Ocean to atmospheric forcing, *J. Phys. Oceanogr., 5,* 572–584, 1975.

Wyrtki, K., and G. Meyers, The trade wind field over the Pacific Ocean, *J. Appl. Meteorol., 15,* 698–704, 1976.

Zuta, S., D. Enfield, J. Valdivia, P. Lagos and C. Blandin, Aspectos fisicos del fenómeno 'El Niño' 1972–73 in *Actas de la Reunion de Trabajo sobre el Fenómeno Conocido como 'El Niño,'* U.N. FAO, Rome, 1976.

(Received May 20, 1980;
revised September 8, 1980;
accepted September 15, 1980.)